© 2023. Published by The Company of Biologists Ltd | Journal of Experimental Biology (2023) 226, jeb244710. doi:10.1242/jeb.244710

RESEARCH ARTICLE

Polarization sensitivity and decentralized visual processing in an animal with a distributed visual system

Daniel R. Chappell* and Daniel I. Speiser

ABSTRACT

The marine mollusc *Acanthopleura granulata* (Mollusca; Polyplacophora) has a distributed visual array composed of hundreds of small image-forming eyes embedded within its eight dorsal shell plates. As in other animals with distributed visual systems, we still have a poor understanding of the visual capabilities of *A. granulata* and we have yet to learn where and how it processes visual information. Using behavioral trials involving isoluminant looming visual stimuli, we found that *A. granulata* demonstrates spatial vision with an angular resolution of 6 deg. We also found that *A. granulata* responds to looming stimuli defined by contrasting angles of linear polarization. To learn where and how *A. granulata* processes visual information, we traced optic nerves using fluorescent lipophilic dyes. We found that the optic nerves innervate the underlying lateral neuropil, a neural tissue layer that circumnavigates the body. Adjacent optic nerves innervate the lateral neuropil with highly overlapping arborizations, suggesting it is the site of an integrated visuotopic map. Using immunohistochemistry, we found that the lateral neuropil of *A. granulata* is subdivided into two separate layers. In comparison, we found that a chiton with eyespots (*Chiton tuberculatus*) and two eyeless chitons (*Ischnochiton papillosus* and *Chaetopleura apiculata*) have lateral neuropil that is a singular circular layer without subdivision, findings consistent with previous work on chiton neuroanatomy. Overall, our results suggest that *A. granulata* effectuates its visually mediated behaviors using a unique processing scheme: it extracts spatial and polarization information using a distributed visual system, and then integrates and processes that information using decentralized neural circuits.

KEY WORDS: Neuroethology, Neuroanatomy, Chiton, Mollusc, Visual ecology, Polarization vision

INTRODUCTION

Animals with distributed visual systems, such as species of cnidarians (Nilsson et al., 2005; Garm et al., 2011), molluscs (Speiser et al., 2011), annelids (Bok et al., 2019) and echinoderms (Garm and Nilsson, 2014; Kirwan et al., 2018; Sumner-Rooney et al., 2018), have arrays of many separate photoreceptive organs dispersed across their bodies. Similar to cephalized visual systems, distributed visual systems include photoreceptive organs that vary in complexity from unpigmented photoreceptors (Ullrich-Lüter et al., 2011) to eyespots (Kingston et al., 2018) to image-forming eyes (Nilsson et al., 2005; Speiser et al., 2011, 2016). Dissimilar to cephalized visual systems, distributed visual systems found in different species vary greatly in their number, arrangement and location of photoreceptive organs. The complex visual information networks that result from these disparate collections of photoreceptive organs are both intriguing and challenging to study, in part because the overall performance of a distributed visual network may be misestimated from the anatomy and physiology of the individual photoreceptive organs that contribute to it. For example, the brittle star *Ophiomastix wendtii* has thousands of dispersed photoreceptors that individually confer coarse directional information about light, but in combination confer spatial vision (Sumner-Rooney et al., 2020).

Because distributed visual systems function as networks, it is vital to characterize them using approaches that illuminate the combined effect of their numerous photoreceptive organs. Top-down behavioral approaches, for example, allow us to investigate representations of higher-order visual information in the nervous systems of animals. Behavioral experiments can reveal these neural representations because visually mediated behaviors reflect integrated visual information rather than input from single photoreceptive organs (Chappell et al., 2021). Additionally, bottom-up neuroanatomical approaches allow us to investigate where and how visual information is integrated and processed, which is largely unknown for many distributed visual systems (Spagnolia and Wilkens, 1983; Garm and Mori, 2009). Thus far, our knowledge of biological visual processing is mostly limited to studies on animals with brains, but some animals with distributed visual systems have relatively decentralized nervous systems without prominent central processing structures. Consequently, investigating the neuroethology of distributed visual systems is likely to uncover novel visual processing schemes.

Chitons (Mollusca; Polyplacophora) are a promising group of animals in which to study the behaviors and neural processing associated with distributed vision (Fig. 1). All chitons are dorsally armored with eight calcified shell plates embedded with extensive networks of small sensory organs termed aesthetes (Moseley, 1885). In some species, these networks include eyespots or eyes (Moseley, 1885; Nowikoff, 1907; Boyle, 1969; Haas and Kriesten, 1978; Speiser et al., 2011). The chiton *Acanthopleura granulata*, for example, has hundreds of small eyes (~80 µm in diameter) embedded within its shell plates (Speiser et al., 2011). Each eye has a retina of ~100 photoreceptors, a layer of screening pigment and an image-forming lens made of aragonite (Speiser et al., 2011, 2014; Li et al., 2015). Like most chitons, *A. granulata* responds defensively to appearances of dark overhead stimuli by lowering its body and clamping to the substrate. Computational models suggest the individual eyes of *A. granulata* provide spatial vision with an angular resolution of 6–9 deg, but behavioral trials exploiting the defensive clamping response of this species have only provided coarse estimates of the angular resolution provided by its network of

Department of Biological Sciences, University of South Carolina, 715 Sumter Street, Columbia, SC 29208, USA.

*Author for correspondence (daniel.r.chappell@gmail.com)

D.R.C., 0000-0003-2214-9335; D.I.S., 0000-0001-6662-3583

Received 14 July 2022; Accepted 19 January 2023

Journal of Experimental Biology (2023) 226, jeb244710. doi:10.1242/jeb.244710

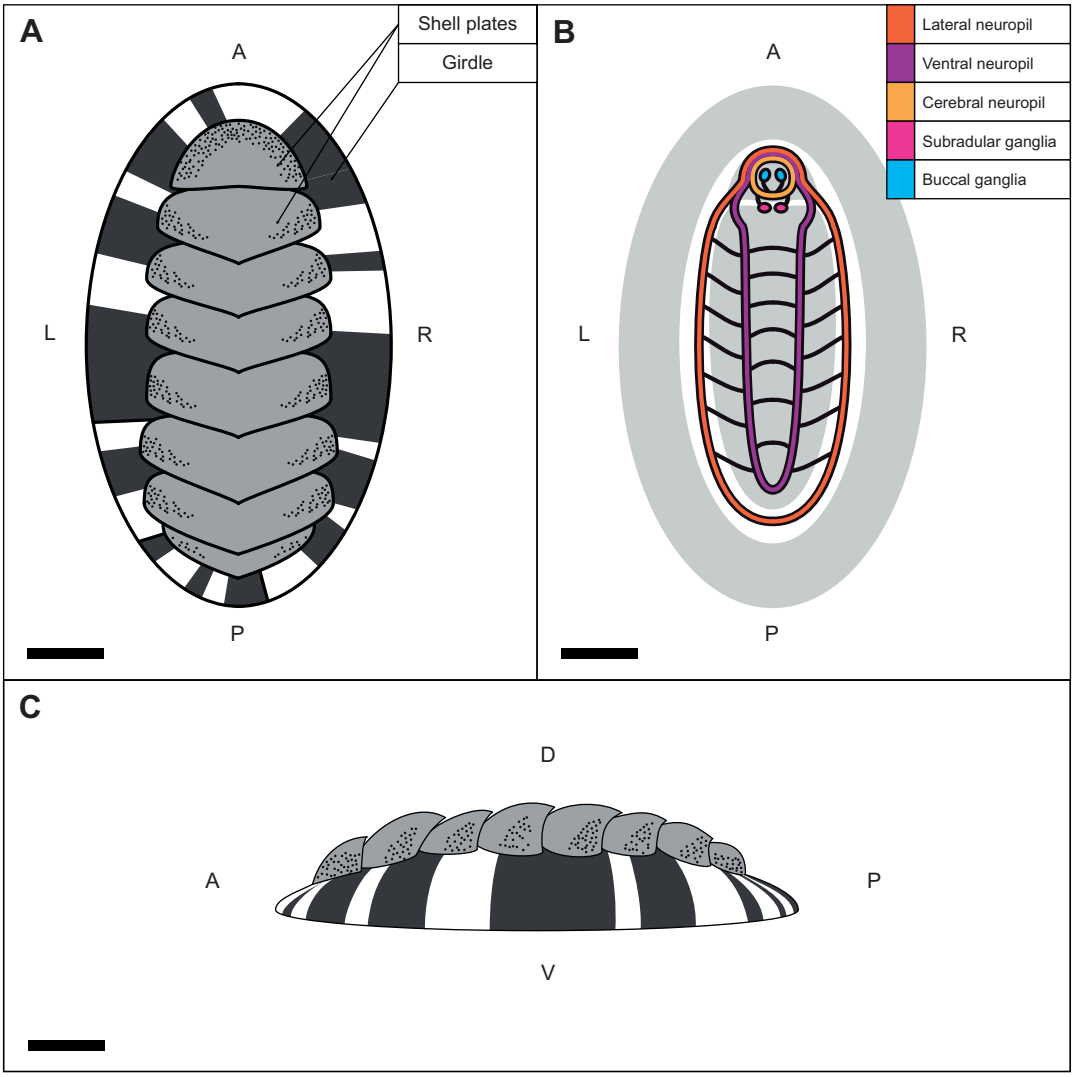

Fig. 1. Illustrations of the anatomy of the chiton *Acanthopleura granulata*. (A) Dorsal view of *A. granulata* showing the eight overlapping shell plates and the black-and-white striped girdle tissue that characterizes this species. The small black dots on the shell plates represent the shell eyes. (B) A schematic of the chiton nervous system, shown from a ventral view and redrawn from Sumner-Rooney and Sigwart (2018). For reference, the girdle, foot and mouth are displayed as gray silhouettes. The major neural structures are color-coded as indicated in the key. (C) Lateral view of *A. granulata* showing the eight overlapping shell plates and the surrounding girdle. Body axes are indicated as anterior–posterior (A–P), dorsal–ventral (D–V) and right–left (R–L). Scale bars: (A–C) 500 µm.

eyes (Speiser et al., 2011; Li et al., 2015). Further, these behavioral trials have not explored polarization sensitivity in *A. granulata*. The photoreceptors in the retinas of eyed chitons, such as *A. granulata*, do not appear to be arranged orthogonally (Boyle, 1969; Speiser et al., 2011), which rules out a common mechanism by which eyes achieve polarization sensitivity (Marshall and Cronin, 2011). Nevertheless, *A. granulata* may still be polarization sensitive because its aragonitic lenses are birefringent and focus incident light of different angles of linear polarization (AoLP) at different positions relative to each underlying retina (Speiser et al., 2011; Li et al., 2015).

We have yet to learn how chitons with eyes, such as *A. granulata*, process visual information. Chitons have nervous systems without prominent ganglia and thus lack the centralized optic lobes canonically associated with vision (Hubrecht, 1882; Sumner-Rooney and Sigwart, 2018). Instead, their nervous systems are predominantly structured by three concentric continuous loops of neuropil that are located within medullary cords (Fig. 1B). These medullary cords travel separately throughout most of the chiton body, but fuse at the anterior end (Hubrecht, 1882; Sumner-Rooney and Sigwart, 2018). Previous anatomical descriptions suggest that the nerves from the aesthetes exit the shell plates and go towards the lateral neuropil, but it is unknown whether these nerves fasciculate with or terminate within the lateral neuropil (von Knorre, 1925). The lack of large centralized ganglia in chitons suggests that visual processing in eyed species takes place within their medullary cords, which would be an unusual and intriguing visual processing scheme.

In this paper, we explored the visually mediated behaviors and neuroanatomy of the eyed chiton *A. granulata*. To investigate the visual capabilities of *A. granulata*, we conducted behavioral experiments that used the innate defensive clamping response of this species as a behavioral readout of its ability to detect different visual stimuli. We tested the angular resolution of spatial vision in *A. granulata* using luminance contrast stimuli that loomed against checkerboard backgrounds of different spatial frequencies. We

tested polarization sensitivity using similar behavioral trials in which looming stimuli and static backgrounds contrasted in terms of AoLP. To identify the location of visual integration within the nervous system of *A. granulata* and characterize its topography, we traced optic nerves using fluorescent lipophilic dyes and imaged them using confocal microscopy. Next, we used fluorescence immunohistochemistry to investigate the tissue substructure at the site of optic nerve innervation in *A. granulata* and then for comparison, repeated this procedure with a chiton species with eyespots (*Chiton tuberculatus*) and two eyeless chiton species (*Ischnochiton papillosus* and *Chaetopleura apiculata*).

MATERIALS AND METHODS

Specimen collection and care

We collected *Acanthopleura granulata* (Gmelin 1791) from a sea wall near Tavernier, FL, USA (25.00N, 80.53W). For behavioral trials, we held specimens in buckets filled with actively aerated natural seawater (NSW). Following the behavioral trials, we transported the animals to the University of South Carolina (Columbia, SC, USA), where we kept them in a Living Stream System (Frigid Units, Toledo, OH, USA) with recirculating NSW held at a temperature of 19.5°C and a salinity of 33 ppt. For lighting, we used two Hydra TwentySix HD LED fixtures (AquaIllumination, Ames, IA, USA) set to a 12 h:12 h light:dark cycle.

We collected *Chiton tuberculatus* Linnaeus 1758 from rocky shores on the island of St Thomas, United States Virgin Islands, using an Indigenous Species Research, Retention and Export Permit (DFW16025U). Following collection, we transported animals to the University of the Virgin Island's MacLean Marine Science Center, where we kept them in a shaded outdoor flow-through sea table supplied with NSW from Brewers Bay.

We acquired *Chaetopleura apiculata* (Say 1834) and *Ischnochiton papillosus* (Adams 1845) from Gulf Specimen Marine Laboratory (Panacea, FL, USA) and housed them at the University of South Carolina (Columbia, SC, USA) in the same Living Stream System and under the same conditions as described above for *A. granulata*.

Equipment and procedures for behavioral experiments

We measured the angular resolution of spatial vision and tested for polarization sensitivity in *A. granulata* using behavioral experiments (Movie 1). In the first experiment, we tested for spatial and polarization vision when animals were submerged in water, and in the second, we tested animals when they were in air. We tested 60 individuals in total, and used 30 individuals for each of the experiments. In trials with submerged animals, we filled a clear plastic 10×10×3 cm container (AMAC Plastic Products, Sonoma Country, CA, USA) to a depth of 3 cm with NSW, placed into the container a smooth piece of 10×10×0.5 cm slate (that had been kept in the same holding container as the test animals), and then placed a single chiton onto the middle of the piece of slate. For trials with animals in air, we followed similar procedures, but did not fill the plastic container with NSW. In each trial, we positioned the container holding the test animal inside a metal frame, set an LCD monitor face down on top of the frame so that the surface of the screen was 20 cm above the test animal, and then draped a sheet of black felt over the metal frame and monitor. We observed and recorded the behaviors of test animals using two Logitech HD C615 webcams that were mounted on tripods, positioned on adjacent sides of the clear plastic container and connected to a computer.

In each trial in our two experiments, we presented a chiton with a series of eight different visual stimuli that were ordered randomly for each test animal. Before presenting visual stimuli to a chiton, we waited for it to begin crawling along the slate substrate. Acclimation by a chiton to the behavioral arena usually took less than 1 min. If a chiton responded to a stimulus, we presented a new stimulus after it resumed crawling (Movie 1). If a chiton did not respond to a stimulus, we presented the next stimulus after a several-second delay. If a chiton either crawled up the walls of the plastic cube or off the slate, we repositioned it back onto the middle of the slate and provided an additional acclimation period before resuming the trial.

The eight visual stimuli that we presented to each chiton included six luminance contrast stimuli and two polarization contrast stimuli (Fig. 2). We displayed luminance contrast stimuli with an unmodified LCD monitor (model E1913Sf, Dell Inc., Round Rock, TX, USA) and polarization contrast stimuli with a modified LCD monitor (model E198FPf, Dell) from which we had removed the front polarizing filter. By making this modification, we could create and display looming stimuli in which the looming circle and the static background contrasted in terms of linear polarization (i.e. different AoLP) instead of luminance contrast (i.e. black versus white). We made and displayed visual stimuli using custom written code in GNU Octave that utilized the Psychophysics Toolbox (Brainard, 1997). We followed established methods to measure the linear polarization contrast of the output of the modified LCD monitor (Pignatelli et al., 2011). Briefly, we measured the irradiance of the screen when it was covered by a linear polarizing filter positioned at relative angles of 0, 45, 90 and 135 deg. We quantified irradiance using a portable fiber-optic spectrophotometer system from Ocean Optics (Dunedin, FL, USA) that included a FLAME-S-VIS-NIR-ES spectrometer, a QP400-1-UV-VIS optical fiber and a CC-3 cosine corrector. We used these irradiance values to calculate the normalized Stokes parameters (S_0, S_1, S_2 and S_3) from which we calculated the AoLP for the 'black' and 'white' states of the modified LCD monitor and the linear contrast comparing these two states. Intensity artifacts can confound behavioral tests of polarization vision, which we accounted for by minimizing surface reflections and preventing large incident viewing angles of the polarized stimuli by showing stimuli in the center of the screen and constraining chitons to a small behavioral arena directly below where stimuli appeared on the screen.

To test spatial resolution in *A. granulata*, we recorded the responses of animals to looming gray circles shown against four different black-and-white checkerboard backgrounds (Fig. 2A–D). These backgrounds consisted of square checks with angular widths of 1.5, 3.0, 4.5 or 6.0 deg (as viewed from the positions of chitons in our behavioral experiments). For brevity, we hereafter refer to these four stimuli as '1.5 deg checker loom', '3.0 deg checker loom', '4.5 deg checker loom' and '6.0 deg checker loom'. We chose this range of angular widths for the checks because morphological estimates of visual acuity suggest that the 1.5 deg checkerboard is too fine for the eyes of *A. granulata* to resolve, whereas the 6.0 deg checkerboard is likely coarse enough to be resolved (Speiser et al., 2011; Li et al., 2015). We chose a gray value for the looming circle that was isoluminant to the overall irradiance of the black-and-white checkerboard backgrounds. By using this gray value for the looming circle, the overall irradiance experienced by animals from the screen remained constant as the looming circle increased in size. The looming circles began with an angular size of 0 deg and over 4.0 s increased to an angular size of 80 deg, which was an angular velocity validated in preliminary trials to elicit strong responses from chitons.

Journal of Experimental Biology (2023) 226, jeb244710. doi:10.1242/jeb.244710

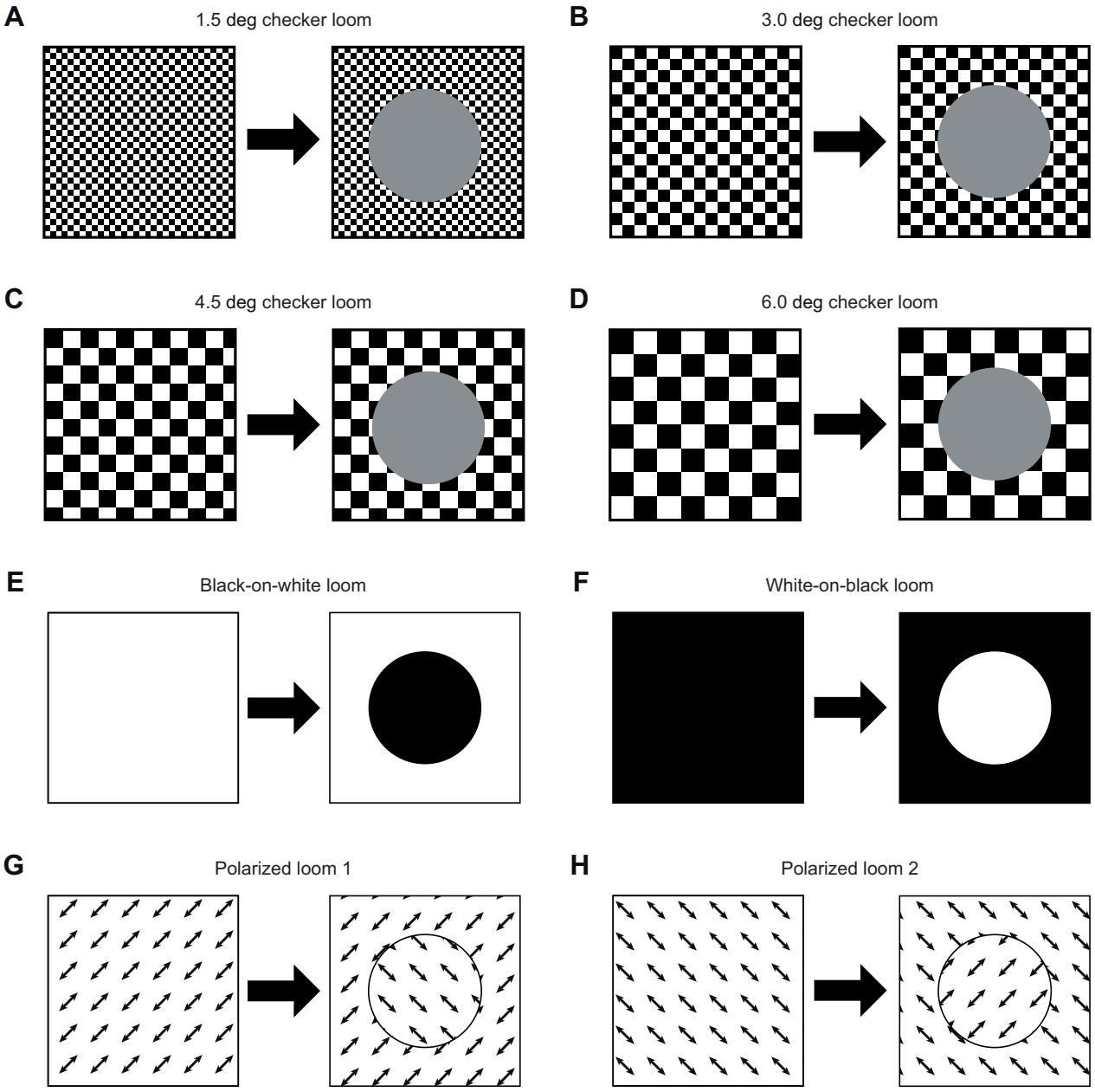

Fig. 2. A schematic overview of the different looming visual stimuli used for the behavioral trials in this study. For each panel, the square on the left represents how a visual stimulus first appears on the screen, and the square on the right represents how the visual stimulus appears at the end of the dynamic loom (which took 4 s in all cases). (A–D) The spatial resolution trial stimuli each had a central looming isoluminant gray circle, but varied in the angular sizes of the squares that composed their background checkerboard patterns. The angular sizes of these squares (as viewed by animals in the behavioral experiments) varied from (A) 1.5 deg, (B) 3.0 deg, (C) 4.5 deg to (D) 6.0 deg. (E–H) The polarization trial stimuli all had a central looming circle, but varied in terms of the color of the circle, the color of the background and the type of screen on which they were shown. (E) The 'black-on-white loom' stimulus consisted of a black circle looming on a white background shown on a normal LCD screen. (F) The 'white-on-black loom' stimulus consisted of a white circle looming on a black background shown on a normal LCD screen. (G,H) The polarized loom stimuli were shown on a modified LCD monitor which displays LCD black and white states as different angles of linear polarization (AoLP), such that images normally contrasting in luminance (i.e. black or white) will instead vary in terms of their AoLP and will be uniformly isoluminant. (G) The 'polarized loom 1' stimulus consisted of a linearly polarized circle looming on a linearly polarized background which varied in terms of its AoLP. (H) The 'polarized loom 2' stimulus consisted of a linearly polarized circle looming on a linearly polarized background which varied in terms of its AoLP. The background of 'polarized loom 1' and the looming circle of 'polarized loom 2' had the same AoLP, and the looming circle of 'polarized loom 1' and the background of 'polarized loom 2' had the same AoLP.

To test for polarization sensitivity in *A. granulata*, we recorded the responses of animals to an additional four types of overhead looming stimuli (Fig. 2E–H). The first two stimuli were luminance contrast and were shown on the unmodified LCD monitor, and the second two stimuli were polarization contrast and were shown on the modified LCD monitor. All stimuli consisted of a uniform background over which a uniform circle of different intensity or AoLP loomed. The looming circles began with an angular size of 0 deg and over 4.0 s increased to an angular size of 80 deg. The first luminance contrast stimulus consisted of a white background with a black looming circle (i.e. 'black-on-white loom') and the second luminance contrast stimulus consisted of a black background with a

white looming circle (i.e. 'white-on-black loom'). The two polarization contrast stimuli were the same as the black-on-white loom and white-on-black loom, but they were displayed on the polarization contrast screen so 'black' and 'white' states differed in AoLP rather than luminance. For brevity, we refer to the black-on-white loom stimulus displayed on the polarization contrast screen as 'polarization loom 1', and the white-on-black stimulus displayed on the polarization contrast screen as 'polarization loom 2'.

Behavioral trial analysis

After conducting behavioral trials, we used our video recordings to score the behavioral responses of chitons to stimuli. To remove bias during the scoring process, we were blind to the order of the visual stimuli presented to chitons in the videos. Following precedent set by previous chiton behavioral studies, we scored a chiton's behavioral response to a stimulus as positive if it lowered its body to the substrate and/or ceased crawling within 2 s of the stimulus being presented (Speiser et al., 2011; Kingston et al., 2018). We separately analyzed the results of the two experiments (the first conducted with animals in water and the second with animals in air).

To analyze our behavioral trial results, we generated and interrogated logistic regression generalized mixed-effect models in R using the lme4 package (Bates et al., 2015). We chose this approach because of the repeated measures design of our experiments (i.e. chitons in both experiments saw all eight of the visual stimuli in random order) and because our dependent variable was binary (i.e. chitons either responded or did not). Our models were of the form: behavioral response∼1+stimuli+(1|chiton individual). We set the responses of animals to the 1.5 deg checker loom as the reference level for our models, a value chosen because morphological estimates of the spatial resolution of individual eyes suggest that this is too fine a pattern for *A. granulata* to resolve (Speiser et al., 2011; Li et al., 2015).

To assess whether the responses of *A. granulata* to the test stimuli differed from their responses to the reference stimulus, we generated logistic odds ratios (LOR) of the response variable for each of the stimuli with confidence intervals (CI). Our models were logistic regression models, so we considered the responses of *A. granulata* to the test stimuli significantly different from the reference level if the LOR CI did not encompass zero. Additionally, we interpreted stimuli with positive LOR as being more likely to trigger behavioral responses by *A. granulata* than the reference stimulus, and those with negative LOR as being less likely to trigger behavioral responses by *A. granulata* than the reference stimulus.

Specimen preparation for morphological analysis

To preserve specimens of *A. granulata*, *C. tuberculatus*, *C. apiculata* and *I. papillosus* for morphological examinations, we fixed whole animals overnight at 4°C in 4% paraformaldehyde in NSW that had been passed through a 0.22 µm syringe filter. We washed fixed specimens three times for 5 min each in filtered NSW and stored them in 0.1 mol l^{-1} phosphate-buffered saline (PBS; 1× PBS, diluted from a 10 PBS stock; Corning, NY, USA) at 4°C. Next, we decalcified the whole, fixed specimens by immersing them in 0.5 mol l^{-1} EDTA (pH 8.0) for ∼2–7 days on a rocker at room temperature. After decalcification, we washed whole specimens 3 times for 10 min in 1× PBS, after which we stored them in 1× PBS at 4°C.

Optic nerve tracing

To trace the optic nerves of *A. granulata*, we used the lipophilic dyes DiI and DiD (Invitrogen, Waltham, MA, USA), which readily incorporate into and diffuse along living or fixed cell membranes. First, we used a micropipette puller (P-1000, Sutter Instruments, Novato, CA, USA) to create fine-tipped thin-walled glass capillary tubes. Then, we partially filled the capillary tubes with a small quantity of either DiI or DiD. We attached the partially filled capillary tubes to a picoliter injection system (PLI-100, Medical System Corporation, Greenvale, NY, USA), which we used to inject a bolus of DiI or DiD into the retinal cups of chosen eyes from fixed and decalcified *A. granulata* specimens. After dye injections, we incubated chiton samples at 4°C for 2 weeks to allow time for DiI or DiD to diffuse along the entire extent of optic nerves. We incubated larger specimens for longer time periods to account for the increased diffusion distances owing to the ontogenetic scaling of their optic nerves.

Next, we embedded specimens in a gelatin-based medium (4% gelatin, 25% bovine serum albumin in 1× PBS) and then fixed the gelatin blocks containing the specimens overnight at 4°C in 4% paraformaldehyde in 1× PBS in foil. We then used a vibratome (Vibratome 1000 Plus Sectioning System, Harvard Apparatus, Holliston, MA, USA) to cut the gelatin-embedded samples into 100 µm thick sections, which we collected and stored in 1× PBS in 24-well plates covered in aluminum foil at 4°C. Finally, we mounted sections onto slides using Fluormount-G (Southern Biotech, Birmingham, AL, USA) and sealed coverslips over them using nail polish.

Immunohistochemistry

To visualize the structure of the lateral neuropil of *A. granulata*, *C. tuberculatus*, *C. apiculata* and *I. papillosus*, we used immunohistochemistry. We performed all of the following steps at room temperature (∼20°C) on a rocker unless otherwise specified. For immunolabeling, we followed the fixation, decalcification and sectioning procedures described above. Next, we dehydrated and rehydrated sections through a series of ethanol–1× PBS solutions for 10 min each as follows: 30%, 50%, 70%, 90%, 100%, 90%, 70%, 50%, 30% and 0%. Then, we permeabilized sections in a series of three 10-min washes of 1× PBS with 0.3% Triton X-100 (PBS-TX). Next, we blocked sections for 1 h in PBS-TX with 5% (v/v) normal goat serum and 2% (w/v) bovine serum albumin (blocking buffer). We then incubated the sections at 4°C for three nights in primary antibodies diluted in blocking buffer as follows: anti-alpha-tubulin raised in mouse (1:500; T5168, Sigma-Aldrich, St Louis, MO, USA) and anti-FMRFamide raised in rabbit (1:1000; NB100-1661, Novus Biologicals, Littleton, CO, USA). We included secondary-only controls, which we did not incubate with primary antibodies but otherwise treated identically. Next, we washed the sections 3 times for 1 h in 1× PBS. For secondary labeling, we incubated sections at 4°C in secondary antibody diluted in blocking buffer (1:400) with added DAPI (1:1000; 4′,6-diamidino-2-phenylindole, Thermo Fisher Scientific, Waltham, MA, USA). The secondary antibodies we used for anti-alpha-tubulin and anti-FMRFamide were goat anti-mouse Alexa Fluor 633 (A-21052, Invitrogen) and donkey anti-rabbit Alexa Fluor 488 (A32790, Alexa Fluor), respectively. We covered the sections with aluminum foil, and incubated them on a rocker for two nights. After immunolabeling, we mounted sections using Fluormount-G (Southern Biotech, Birmingham, AL, USA) and sealed the coverslips using nail polish.

Confocal imaging and image processing

To image the fluorescently labeled tissue sections produced from both the optic nerve tracing and the immunohistochemistry experiments

Journal of Experimental Biology (2023) 226, jeb244710. doi:10.1242/jeb.244710

described above, we used a Leica SP8 X confocal microscopy system (Leica Microsystems, Buffalo Grove, IL, USA), with a water immersion 40× objective (NA 1.10). We collected most images at 1024×1024 pixels, but for some samples we used the integrated tile scanning ability of the Leica SP8X microscope to obtain larger panoramic images. For fluorophore excitation, we used a 405 nm diode laser (120 mW, 20% power) to excite DAPI, and used a white-light laser (500 mW, 50% power) to excite all other fluorophores, including DiI and DiD. For the secondary-only and untreated controls, we used the same acquisition parameters as the corresponding treatment samples. We then used FIJI (Schindelin et al., 2012) to process the images in a variety of ways, including creating maximum projections of *z*-stacks, forming composite images from multiple color channels and forming panoramic images from tile-scans. Additionally, we used the 3DViewer plugin in FIJI to construct 3D volumetric models from the confocal *z*-stacks and to create video animations of these models (Schmid et al., 2010).

RESULTS

Acanthopleura granulata demonstrates spatial vision with an angular resolution of 6 deg

As a measure of spatial resolution, we estimated the minimum resolvable angle (α_{min}) in *A. granulata* to be 6 deg, twice the width of the narrowest squares that it was able to resolve (3 deg). We found that a greater number of *A. granulata* responded to looming stimuli against coarser checkerboard backgrounds. In our first experiment, in which animals were submerged in water, the proportion of chitons that responded to each of the stimuli were as follows: 1/30 chitons for the 1.5 deg checker loom, 12/30 for the 3.0 deg checker loom, 24/30 for the 4.5 deg checker loom and 29/30 for the 6.0 deg checker loom (Fig. 3A). In our second experiment, in which animals were in air, the proportion of chitons that responded to each of the stimuli were as follows: 1/30 chitons for the 1.5 deg checker loom, 13/30 for the 3.0 deg checker loom, 27/30 for the 4.5 deg checker loom and 28/30 for the 6.0 deg checker loom (Fig. 3B).

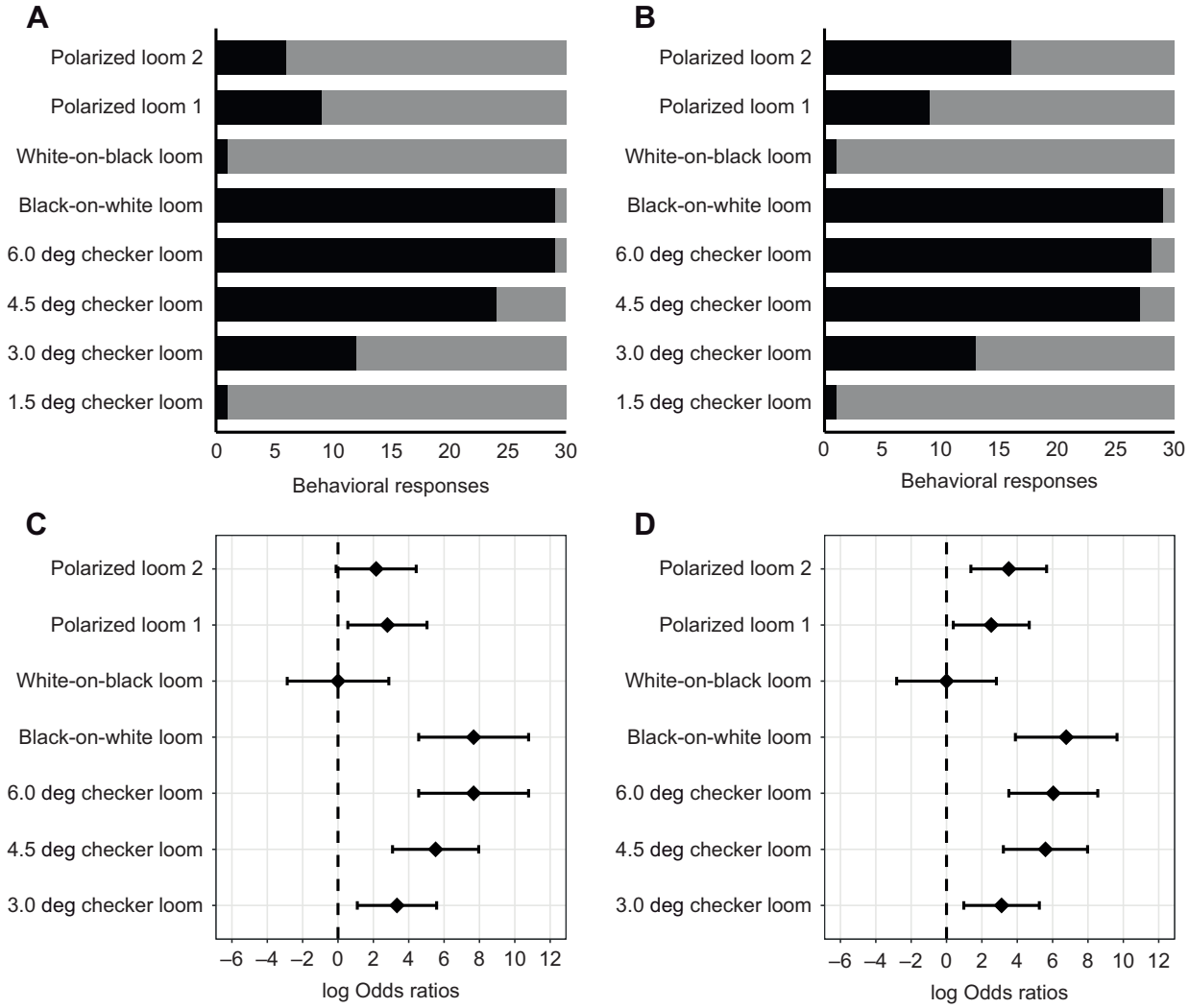

Fig. 3. The proportion of *Acanthopleura granulata* individuals that responded to each of the visual stimuli and the log odds ratios of the behavioral responses compared with the reference level (response to the 1.5 deg checker loom). (A,B) Stacked horizontal bar charts showing the proportion of *A. granulata* individuals that responded to a stimulus (black section) or did not respond to the stimulus (gray section). The proportion of responses to all of the stimuli are displayed in separate bar charts for trials conducted in water (A) and trials conducted in air (B). (C,D) Plots showing the mean log odds ratio (black diamonds) with confidence intervals of positive behavioral responses of *A. granulata* for each of the visual stimuli presented in water (C) or in air (D). In this plot, log odds ratios greater than zero represent higher odds of a positive behavioral response to a stimulus compared to the reference stimulus (i.e. 1.5 deg checker loom), and log odds ratios less than zero represent lower odds of a positive behavioral response to a stimulus compared with the reference stimulus.

Journal of Experimental Biology (2023) 226, jeb244710. doi:10.1242/jeb.244710

Using the LOR generated by our generalized linear mixed-effect models, we found that in water, *A. granulata* was significantly likely to respond to the 3.0 deg checker loom (LOR CI, 1.1:5.5), the 4.5 deg checker loom (LOR CI, 0.7:5.5) and the 6.0 deg checker loom (LOR CI, 4.6:10.8) (Fig. 3C). In air, we similarly found that *A. granulata* was significantly likely to respond to the 3.0 deg checker loom (LOR CI, 1.0:5.2), the 4.5 deg checker loom (LOR CI, 3.2:8.0) and the 6 deg checker loom (LOR CI, 3.5:8.5) (Fig. 3D).

Acanthopleura granulata is polarization sensitive

We found that *A. granulata* responds to looming stimuli defined by contrasting AoLP. In water, the proportion of chitons that responded to each of the looming stimuli shown against uniform backgrounds were as follows: 29/30 chitons responded to the black-on-white loom, 1/30 chitons responded to the white-on-black loom, 9/30 chitons responded to polarization loom 1 and 6/30 chitons responded to polarization loom 2 (Fig. 3A). In air, the proportion of chitons that responded to each of the stimuli were as follows: 29/30 chitons responded to the black-on-white loom, 1/30 chitons responded to the white-on-black loom, 9/30 chitons responded to polarization loom 1 and 16/30 chitons responded to polarization loom 2 (Fig. 3B). Across trials, the looming polarized stimuli elicited positive behavioral responses when they reached similar angular sizes: 34.4±6.8 deg for polarization loom 1 in water, 32.2 ±7.1 deg for polarization loom 1 in air, 37.5±7.6 deg for polarization loom 2 in water and 35.0±7.9 deg for polarization loom 2 in air. A stimuli incident angle of 15 deg is an acceptable deviation from perpendicular viewing and well within the viewing conditions commonly employed for behavioral polarization tests.

Using the LOR generated by our generalized linear mixed-effect models, we found that in water, *A. granulata* was not significantly likely to respond to the white-on-black loom (LOR CI, –2.9:2.9) or to polarization loom 2 (LOR CI, –0.10:4.42), but was significantly likely to respond to the black-on-white loom (LOR CI, 4.6:10.8) and polarization loom 1 (LOR CI, 0.6:5.0) (Fig. 3C). In air, we found that *A. granulata* was not significantly likely to respond to the white-on-black loom (LOR CI, –2.8:2.8), but was significantly likely to respond to the black-on-white loom (LOR CI, 3.9:9.7), polarization loom 1 (LOR CI, 0.4:4.6) and polarization loom 2 (LOR CI, 1.4:5.6) (Fig. 3D).

Optic nerves of *A. granulata* innervate the lateral neuropil to form a visuotopic map

The optic nerves of *A. granulata* take elaborate pathways to connect the eyes in the shell plates with the rest of the nervous system. Lipophilic dyes injected into each eye cup diffused into the cellular membranes of photoreceptors, and laterally diffused within the membranes to trace the ventrally projected neurite extending from each photoreceptor (i.e. optic neurites). Ventral to each retina, the optic neurites fasciculate into a dense optic nerve, one of which travels laterally from each eye to the edge of the shell plate in which the eye is embedded. To reach the edge of a shell plate, an optic nerve passes through the otherwise dense mineralized shell material via a system of canals (Fernandez et al., 2007). Once a tightly fasciculated optic nerve reaches the lateral edge of a shell plate, its optic neurites defasciculate from one another to form an irregular neural plexus (Fig. 4; Movie 2). These neural plexuses are located within the perforated mineralized matrices at the lateral margins of each shell plate (i.e. 'spongy eaves'), which are the active sites for new shell growth. On the ventral side of a plexus, the optic neurites fasciculate again to form consolidated optic nerves, which subsequently bunch together to form aggregate optic nerves containing neurites from multiple eyes. To pass from the dorsal to ventral side of a shell plate, each aggregate optic nerve travels through one of the shell plate's radially periodic insertion slits (i.e. passages through the articulamentum, the lower of the two layers of shell material). Our observations corroborate previous microdissection investigations that suggest that the insertion slits allow nerves to pass between the insertion plates that anchor the shell plates to the musculature of the girdle tissue (von Knorre, 1925).

We found that the optic nerves of *A. granulata* innervate the lateral neuropil, which is a neural tissue layer that circumnavigates the body (Fig. 1B). After exiting shell plates, optic nerves travel medially to reach the roof of the pallial cavity and then travel superficially and medially until they reach the lateral neuropil. Upon reaching the lateral neuropil, each optic nerve branches into a characteristic H-shaped arborization pattern (Fig. 5; Movie 3). This branching pattern arises from an optic nerve bisecting into two separate neurite bundles followed by each bundle heading towards different mediolateral tracts of the lateral neuropil. Once at their respective tracts, these neurite bundles split again and the neurites travel bidirectionally along the lateral neuropil. Individual optic neurites within the lateral neuropil have periodic varicosities, which give the appearance of beads on a string. We did not observe these varicosities in optic neurites outside of their arborizations along the lateral neuropil.

We found that the optic nerves arborize along the lateral neuropil visuotopically; that is, different radial sections of an animal's visual field are mapped onto different radial sections of its lateral neuropil loop (Fig. 5). Eyes on adjacent shell plates project optic nerves which arborize along adjacent sections of the lateral neuropil, as do eyes on adjacent sections of the same shell plate. In this way, each section of the lateral neuropil loop contains optic nerve arborizations from eyes in the directly overlying shell plates. Additionally, we found that arborizations from separate optic nerves traversed considerable distances along the lateral neuropil to overlap with one another. We observed that the optic neurites from different eyes traversed closely to one another, and did not show evidence of neuronal tiling (i.e. they did not have well-defined arborization boundaries).

The lateral neuropil of *A. granulata* is partially subdivided

The lateral neuropil of *A. granulata* is dorsoventrally flattened and subdivided into two distinct layers by an invaginating vein of neuronal cell bodies (Fig. 6A). In contrast, the lateral neuropil in other chiton species is circular in cross-section and surrounded by a cortex of neuronal cell bodies (Sumner-Rooney and Sigwart, 2018). We corroborated this finding in *C. tuberculatus*, *I. papillosus* and *C. apiculata*, all of which had lateral neuropil consisting of a circular central layer of neuropil surrounded by a dense layer of cell bodies (presumptively neuronal somata) (Fig. 6B–D). The unusual anatomy and subdivision of the lateral neuropil in *A. granulata* is reminiscent of the subdivisions of the lateral, ventral and cerebral neuropil layers within the circumesophageal nerve rings of chitons (Plate, 1897; Sumner-Rooney and Sigwart, 2018). In *A. granulata*, however, such subdivisions are found not only in the circumesophageal nerve ring, but also within the entire lateral neuropil.

Like its lateral neuropil, the anterior commissure of *A. granulata* has more subdivisions than the anterior commissures of other chitons (Fig. 6E,F). The anterior commissure is the anterior half of the circumesophageal nerve ring, a neural structure found in most molluscs that encircles the mouth. In chitons, the anterior

Journal of Experimental Biology (2023) 226, jeb244710. doi:10.1242/jeb.244710

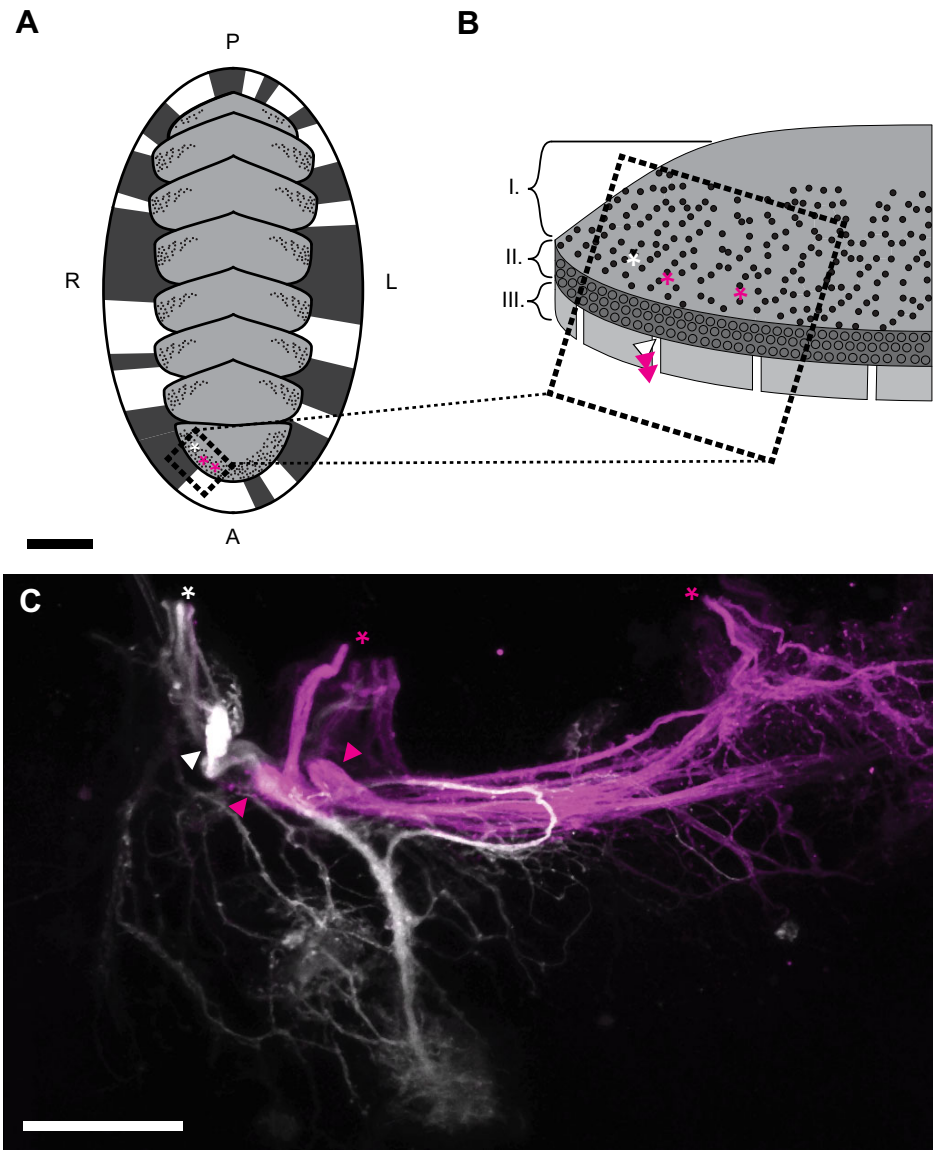

Fig. 4. The neural plexus of optic nerves along the lateral edge of a shell plate from *A. granulata*. (A) An illustration of the dorsal view of *A. granulata* showing the location and pattern of lipophilic dye injections as asterisks. Multiple eyes on adjacent sections of the anterior-most shell plate were injected with different lipophilic dyes (DiI or DiD), which are false colored to be magenta and white, respectively, in C. The black dashed box in A represents the field of view in B. (B) An illustration of the lateral view of the anterior-most shell plate from *A. granulata* again showing the location and pattern of lipophilic dye injections as asterisks. Regions of the shell plate include the dorsal surface (I), the eaves (II) and the insertion plates/slits (III). The black dashed box in B represents the field of view in C. (C) Confocal microscopy image of a frontal section through the lateral margin of the anterior shell plate of *A. granulata* showing multiple fluorescently labeled optic nerves. The optic nerves enter the dorsal side of the sectioning plane (asterisks), and at these locations are still within the canals in the shell plate through which they connect with the eyes. After emerging from the canal system, the optic nerves defasciculate to form an irregular neural plexus. The optic neurites traverse this neural plexus and then fasciculate into large optic nerves (arrowheads) prior to intersecting the ventral sectioning plane. Scale bars: (A) 500 µm, (C) 50 µm.

commissure is formed from the fusion of the lateral, ventral and cerebral neuropil. In most chitons, the three layers of neuropil in the anterior commissure are separated by veins of neuronal cell bodies. In *A. granulata*, however, we see additional neuropil subdivisions within the anterior commissure created by veins of cell bodies, which may indicate additional layers of neuropil. In the region of the lateral neuropil, there is a well-defined subdivision created by a thick boundary of cell bodies. In the region of the cerebral neuropil, we see a less well-defined vein of cell bodies which incompletely divides the neuropil (Fig. 6E,F). As a consequence, the anterior commissure of *A. granulata* appears to contain five neuropil layers, two more than observed in any other chiton to date.

DISCUSSION

Acanthopleura granulata demonstrates spatial vision

Our estimate of the visual spatial resolution of *A. granulata* as 6 deg solid angle aligns with computational estimates of spatial resolution in this species (Speiser et al., 2011; Li et al., 2015). By combining crystallographic techniques, microCT and ray tracing, Li et al. (2015) estimated the angular resolution of the eyes of *A. granulata* to be between 8 and 13 deg in air and between 6 and 9 deg in seawater. These estimates represent a best-case scenario for angular resolution because disorganization of the microvillar projections of photoreceptors (as indicated by Boyle, 1969 for *Onithochiton neglectus*) will coarsen the angular resolution an eye can provide. Our behavioral estimates of visual spatial resolution of 6 deg in both air and seawater suggest *A. granulata* is able to detect visual stimuli right at the edge of the resolvable limit of its individual eyes. In fact, the visual spatial resolution required to discern the checkerboard looms in water is even finer than our estimates because the chitons viewed the stimuli through Snell's window at the water–air interface, which compresses the 180 deg field of view above the water to ∼96 deg below the water.

It is possible that *A. granulata* enhances its visual spatial resolution via leveraging the redundant sampling of visual stimuli by its distributed array of eyes, which have highly overlapping visual fields (Li et al., 2015). Certain points of the surrounding visual field could be sampled by as many as 150 eyes, based on estimates of eye density (∼12 eyes per mm^2), visual field size (60 deg solid angle; Li et al., 2015) and radii of shell surface curvatures (∼2.68 mm radial and ∼5.59 mm dorso-ventral). If so, the visual system of *A. granulata* may function similarly to multi-

Journal of Experimental Biology (2023) 226, jeb244710. doi:10.1242/jeb.244710

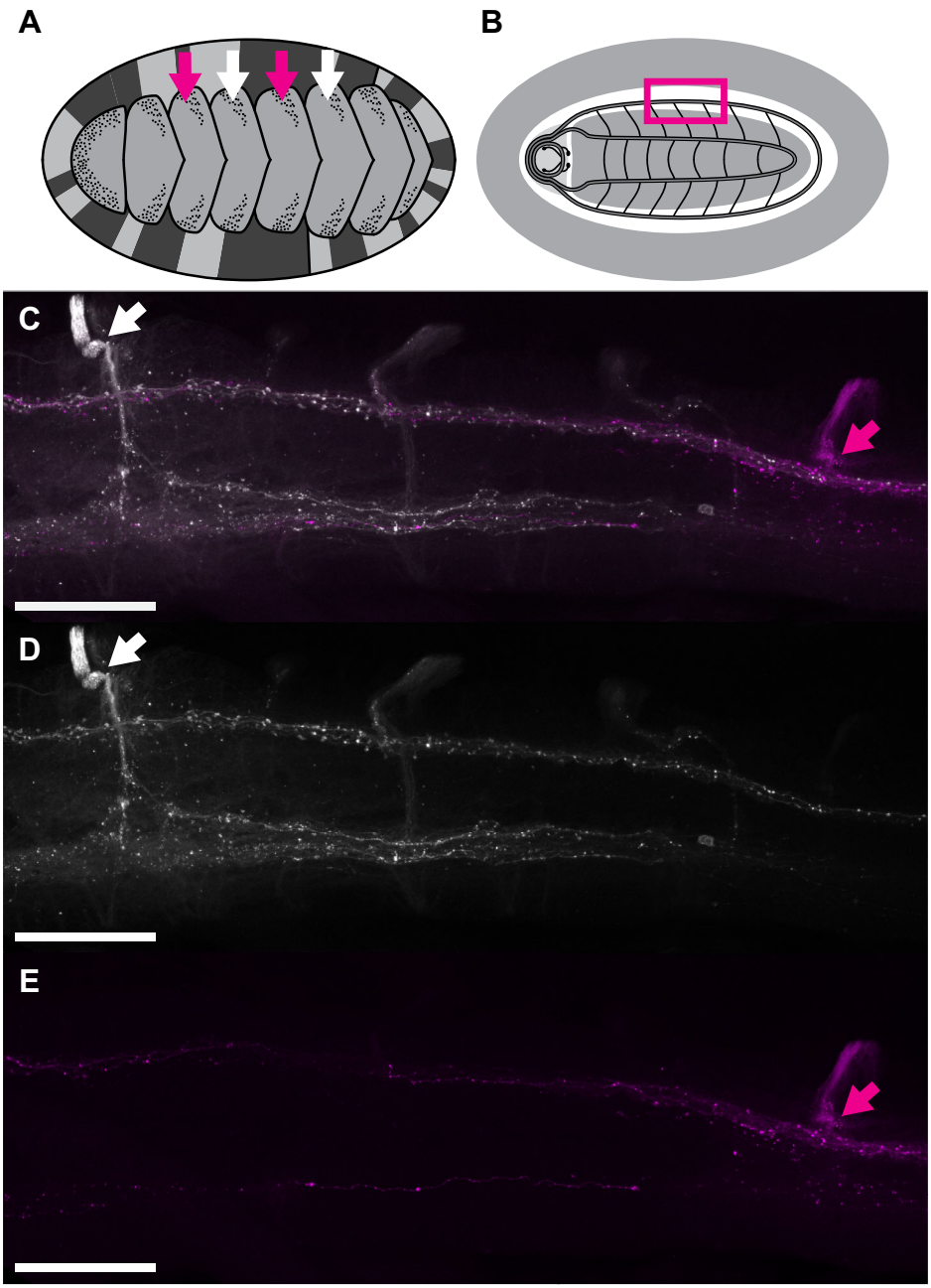

Fig. 5. The pattern of optic nerve arborization along the lateral neuropil of *A. granulata*. (A) An illustration of the dorsal view of *A. granulata* showing the location and pattern of lipophilic dye injections as arrows. Single eyes on alternating shell plates were injected with different fluorescent lipophilic dyes (DiI and DiD), which are false colored to be magenta and white, respectively, in the confocal microscopy images. (B) An illustration of the chiton nervous system showing the approximate field of view for the microscopy images in C–E, which are dorsal views of a frontal section along the lateral neuropil. (C) A confocal microscopy image showing the arborization of two optic nerves along the lateral neuropil which are labeled with different dyes and are shown separately in D and E for clarity. In C, two fasciculated optic nerves, each labeled by an arrow, are seen to split into two separate neurite bundles which travel to separate tracts of the neuropil. The separate neurite bundles then bifurcate again and travel bidirectionally along the lateral neuropil. Scale bars: (C–E) 100 µm.

channel sensor arrays in which the region of interest is sampled simultaneously by multiple sensors so as to overcome the noise limitations of the individual sensors (Larson and Taulu, 2017). The advantage of using spatial oversampling to overcome noise instead of temporal summation is that the detection time window – which is preferably minimized to detect quickly moving predators – would not be increased by longer integration times. Similarly, the advantage of using spatial oversampling to overcome noise instead of spatial summation is that spatial resolution – which is preferably maximized to preserve acuity – would not be coarsened by summing input from neighboring photoreceptors found in the same eye.

The methods we employed for testing spatial vision in *A. granulata* represent a substantial improvement over past efforts. They confirm that *A. granulata* has spatial vision and, for the first time, provide a reliable estimate of its visual spatial resolution. Previous behavioral trials on *A. granulata* found support for spatial vision, but the design of the visual stimuli precluded the ability to interpret visual acuity from the behavioral responses of animals (Speiser et al., 2011). In this earlier study, the authors found that *A. granulata* was more likely to respond to the sudden overhead appearance of a 9 deg solid angle black circle than the appearance of an isoluminant gray screen. The problem with the design of the visual stimuli in this experiment (and others like it) is that the angular size of the black circle does not directly correspond with the angular resolution required to see it. The appearance of the black circle will result in a noticeable drop in radiance for all receptive fields smaller than the whole screen. Therefore, though *A. granulata* was found to respond to a 9 deg solid angle black circle, this stimulus could be discerned from an isoluminant gray screen by an eye with a spatial resolution of 60 deg solid angle or perhaps even coarser.

Journal of Experimental Biology (2023) 226, jeb244710. doi:10.1242/jeb.244710

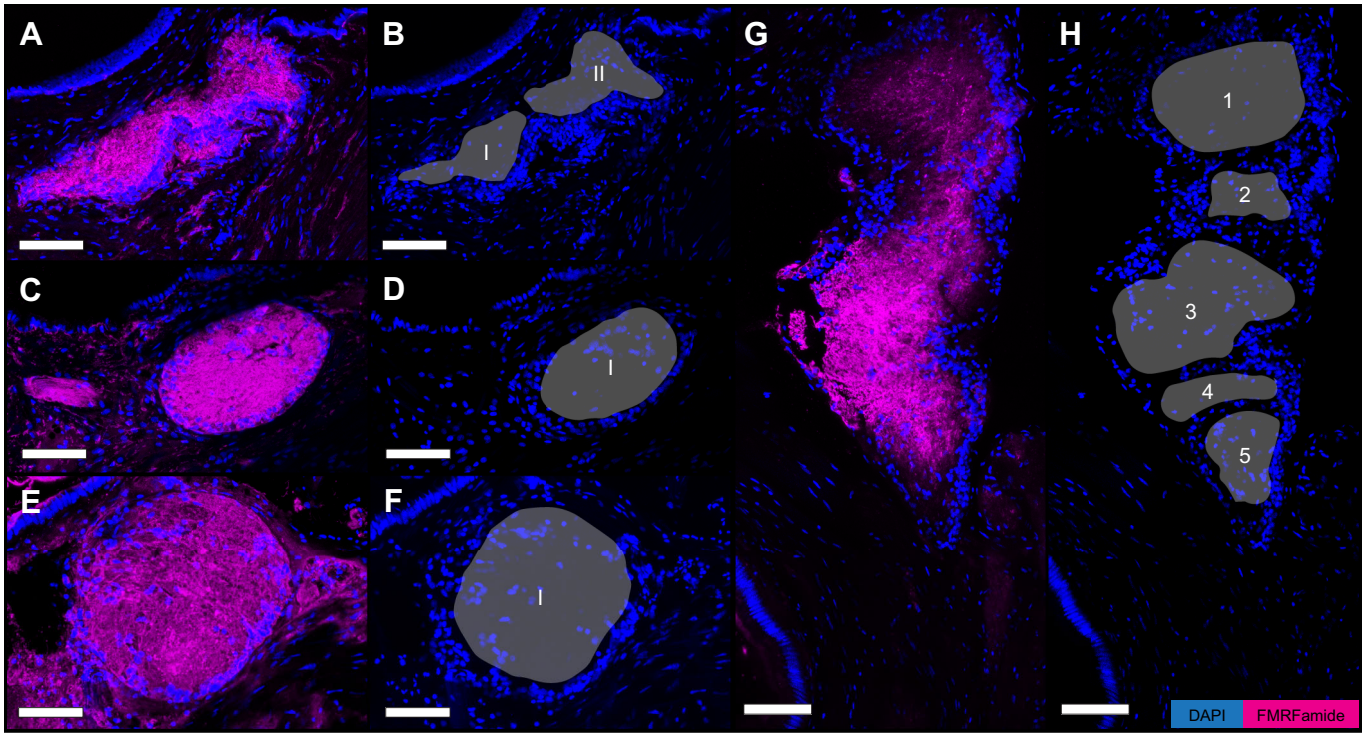

Fig. 6. Neuropil is subdivided into additional layers in *A. granulata* compared with other chitons. In all images, obtained via confocal microscopy, cell nuclei are labeled with DAPI and displayed in blue, and neuropil is labeled with anti-FMRF-amide and displayed in magenta. The images are paired showing the same tissue labeled with (A,C,E,G) DAPI and FMRF-amide, and (B,D,F,H) DAPI alone for clarity with neuropil annotated with roman numerals or numbers. (A–F) Cross-sections of lateral nerve cords from the chiton species (A,B) *Acanthopleura granulata*, (C,D) *Chiton tuberculatus* and (E,F) *Ischnochiton papillosus*. The lateral nerve cord of *A. granulata* (A,B) has a central neuropil layer that is dorsoventrally flattened, and an invaginating vein of cell bodies that largely subdivides the neuropil into two parts (I,II). In comparison, the lateral nerve cords of the other species investigated (C–F) have circular central neuropil layers (I) and outer layers of neuronal cell bodies. (G,H) Cross-section of the anterior half of the circumesophageal nerve ring of *A. granulata*. In most chitons, this cross-section would show only three layers of neuropils, corresponding to the lateral, ventral and cerebral neuropil subdivided by interspersed veins of cell bodies, but in *A. granulata*, we see five layers of neuropil: (1) lateral neuropil, (2) new neuropil layer in *A. granulata*, (3) ventral neuropil, (4) new neuropil layer in *A. granulata* and (5) cerebral neuropil. The neuropil layers 2 and 4 have not been reported in other chitons. Scale bars: (A–H) 50 µm.

The visual stimuli that we displayed in our behavioral trials in this study minimized luminance artifacts by using checkerboard backgrounds over which isoluminant gray circles loomed. Because the background is unchanging and the gray circle is isoluminant, the overall radiant flux emitted by the screen is unchanging despite the looming circle. The threshold receptive field size of individual photoreceptors for which a stimulus is not isoluminant is equal to or less than twice the width of each of the squares that comprise the checkerboard background. Animals whose eyes have photoreceptors with receptive fields smaller than this threshold can visually detect the looming circle. For eyes with photoreceptors whose receptive fields are larger than this threshold, the stimuli design we employed prevents luminance artifacts that could yield inaccurately fine estimates of spatial resolution.

Acanthopleura granulata demonstrates polarization sensitivity

Our results show that *A. granulata* behaviorally responds to AoLP contrasting looming stimuli, which can only be detected using polarization vision. Intriguingly, the retinas of *A. granulata* do not appear to be intrinsically polarization-sensitive like those of other invertebrates that can distinguish AoLP, such as arthropods and cephalopods. Most of these animals achieve polarization vision using rhabdomeric photoreceptors with photoreceptive regions that consist of dense arrays of parallel microvillar extensions. These microvillar arrays are maximally sensitive to light with an e-vector that is aligned with their long axis, making the photoreceptors that bear them maximally sensitive to light of a set AoLP (Marshall and Cronin, 2011). By arranging these microvillar photoreceptors orthogonally and performing opponency processing on their outputs, some arthropods and cephalopods are able to extract the AoLP information from visual scenes (Marshall and Cronin, 2011). Based on morphological descriptions of retinas from other eyed chitons (e.g. *Onithochiton neglectus*; Boyle, 1969), we infer that the photoreceptors in the retinas of *A. granulata* have microvillar extensions, but are organized in radially symmetric arrays. Radially arranged photoreceptors combined with camera-type optics likely make the retinas of *A. granulata* sensitive to a wide range of e-vector angles of light, but preclude polarization vision through any well-established methods.

Without the canonical morphological traits associated with polarization vision, how is *A. granulata* sensitive to AoLP-contrasting stimuli? An intriguing feature of the eyes of *A. granulata* is that their aragonitic lenses are birefringent (Speiser et al., 2011; Li et al., 2015). Aragonite is a pseudo-uniaxial crystal, so the double refraction of an aragonite lens could be minimized by aligning the *c*-axis of the crystalline material with the optical axis of the eye. In fact, the uniaxial calcitic lenses found in the schizochroal eyes of trilobites are oriented in this way, which effectively preserves image contrast by not forming two images simultaneously

(Towe, 1973). A previous study reported that the aragonitic lenses of *A. granulata* have *c*-axes offset from the optical axes of eyes by 45 deg, so the lenses are functionally birefringent and form two images within single eye chambers (Li et al., 2015). This has been interpreted as a potential way for *A. granulata* to keep focused images on their retinas in both air and water, despite having static optical organs that cannot adjust focus by changing lens shape or location, a method for focusing employed by other camera-type eyes (Speiser et al., 2011; Li et al., 2015).

Beyond allowing the eyes of *A. granulata* to form in-focus images in water and air, birefringent lenses will focus light to different focal planes depending on its AoLP. In this way, a birefringent lens may selectively focus features of certain AoLP onto the underlying retina. We currently do not know how the *c*-axes of the lenses of *A. granulata* are aligned with respect to one another, but it is likely that they vary across the network of eyes (Friedrich et al., 2021 preprint). If the eyes were located on a flat surface it would be possible for the *c*-axes of their lenses to be aligned, but this is not the case for the eyes of *A. granulata* because they are located on multi-curvature shell plates. Aligning the *c*-axes of all of these lenses would disrupt the focal distances of individual eyes across the visual array. If *c*-axis orientation was stochastically distributed across the array of lenses, neighboring eyes (which have highly overlapping visual fields) would selectively focus different AoLP features of the same visual scenes. Non-polarized visual features would be detected by all eyes viewing them, whereas linearly polarized visual features would be selectively detected by a subset of eyes. Some eyes will have the *c*-axes of their lenses oriented such that polarized images fall on their retinas, whereas others will have the *c*-axes of their lenses oriented such that polarized images fall either in front of or behind their retinas. Although future studies are required to show proof of this mechanism, it could be a novel approach to polarization vision and a unique benefit of sensing with an array of non-homogenous sensory organs.

We have shown that *A. granulata* achieves polarization sensitivity and likely does so using a novel mechanism: a birefringent lens. However, we have yet to learn whether polarization vision is functionally beneficial to *A. granulata* or whether it is a non-adaptive consequence of their aragonite lenses (i.e. birefringent lenses in chitons may be an optical spandrel; Gould and Lewontin, 1979; Gould, 1997). Many animals with polarization vision use it for tasks such as reducing glare to improve visual contrast, navigating using celestial polarization cues, perceiving polarized sexual signals and detecting water from the air (Marshall and Cronin, 2011). Eyed chitons are thought to use spatial vision to detect predators (Speiser et al., 2011), but it is unclear how polarization vision would help them do so. Some eyed chitons, such as *Acanthopleura gemmata* (Chelazzi et al., 1987), demonstrate homing behaviors that could be aided by polarized celestial cues, such as those used for navigation by certain arthropods (e.g. *Scarabaeus zambesianus*; Dacke et al., 2003). Currently, homing behavior in eyed chitons is thought to be explained by chemical trail following (Chelazzi et al., 1987), but it is common for invertebrates to use multimodal cues when navigating (Buehlmann et al., 2020; Mongeau et al., 2021).

Acanthopleura granulata likely processes visual information using decentralized circuits

Our results demonstrate that the optic nerves of *A. granulata* innervate the lateral neuropil and do not appear to innervate any other neural structure. First, we are confident that the optic neurites terminate in the lateral neuropil and that their arborizations were fully labeled: we observed the same optic nerve arborization patterns across multiple specimens of *A. granulata* that varied in body size and across eyes with different spatial locations on the same shell plates. Seeing similar arborization patterns across preparations suggests complete labeling of optic nerves because the lipophilic dyes we injected into eyes had different diffusion distances in all of these cases. Second, we interpret the periodic varicosities that we observed along optic neurites in the lateral neuropil as synaptic boutons of *en passant* synapses, which are commonly found in molluscan neurons (Petralia et al., 2021). We observed these varicosities in multiple specimens, and did not observe them in the optic neurites outside of their areas of arborization along the lateral neuropil. Molluscan neurons commonly provide and receive synaptic connections along their unipolar neurite arborizations (i.e. they do not have dendrites near their cell bodies), so it is likely the optic neurites in *A. granulata* form synaptic connections with interneuron arborizations located in the lateral neuropil (Ramón y Cajal, 1904).

The optic nerves that innervate the lateral neuropil appear to form a decentralized visuotopic map (Fig. 7). This map is decentralized because the lateral neuropil is a relatively large cordal neural structure that circumnavigates the body, and the optic nerves appear to innervate along its entire extent. If visual information was processed centrally in *A. granulata*, we would expect the optic nerves to target a central location or specific interneurons, as happens for sensory afferents in the spinal cords of vertebrates (Straka et al., 2014). Instead, in *A. granulata*, we see optic nerves targeting broad regions of the lateral neuropil with wide arborizations that travel bidirectionally and seemingly make synaptic connections across the extent of the arborization. If we saw the optic nerve arborizations occupying discrete regions of the lateral neuropil (i.e. if they were non-overlapping), we would conclude that the primary visual map is spatiotopic, where the spatial positions of eyes are mirrored in the positions of their optic nerve arborizations. In this scenario, the visual information from individual eyes would be initially segregated. Instead, we find that the optic nerve arborizations from separate eyes are highly overlapping within the lateral neuropil, which suggests the primary visual map may be visuotopic rather than just spatiotopic. In this scenario, it is regions of the visual field that are initially mapped onto the lateral neuropil, not input from individual eyes (Fig. 7). Because the eyes have wide and highly overlapping visual fields, their optic nerve arborizations must traverse correspondingly large distances of the lateral neuropil to reconstruct regions of visual space, a prediction consistent with our observations.

Visual information is likely processed by *A. granulata* in decentralized circuits within its lateral neuropil because the optic nerves form an extensive decentralized visuotopic map along the entire extent of the lateral neuropil. Decentralized architectures may be common for sensory-motor circuits in chitons: previous experiments have demonstrated decentralized neural control of muscular systems in chitons, including their heart (Matsumura and Kuwasawa, 1996). We predict that the decentralized circuits in the lateral neuropil integrate visual information with information from other sensory modalities to guide motor behaviors. We make this prediction because numerous peripheral sensory organs of non-visual modalities, including non-eye aesthetes, likely project sensory afferents to the lateral neuropil (von Knorre, 1925; Sigwart et al., 2014). The lack of a large central neural structure and the large number of sensory organs suggest chitons integrate sensory information locally. Given the lack of numerous well-defined

Journal of Experimental Biology (2023) 226, jeb244710. doi:10.1242/jeb.244710

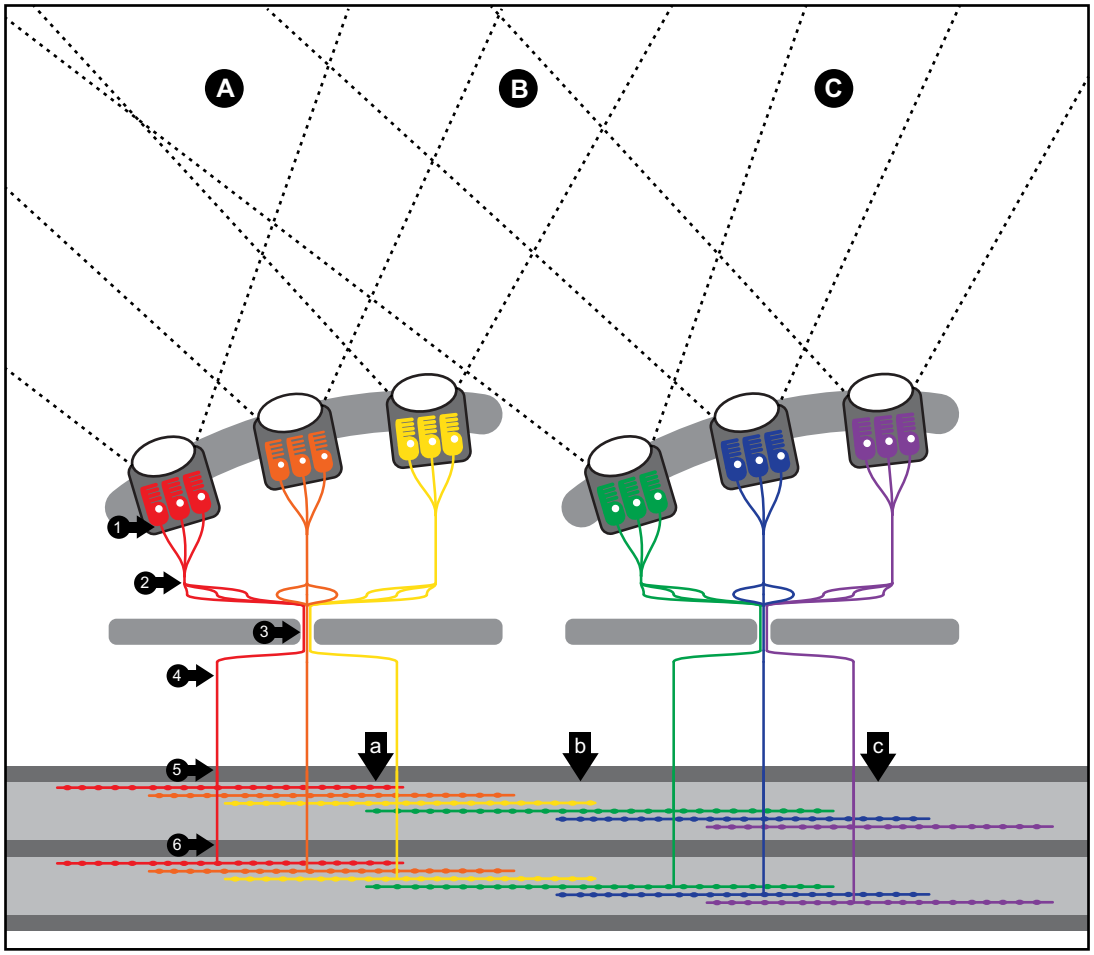

Fig. 7. Model of visual system integration in the eyed chiton *A. granulata*. (1) Each photoreceptor ventrally projects a neurite that fasciculates with other neurites from the same eye to form an optic nerve. (2) The optic nerve travels laterally through a network of channels to reach the edge of the shell plate. The optic nerve emerges from the canal network at the edge of the shell plate and defasciculates with other optic nerves to form a neural plexus. (3) The defasciculated neurites converge and fasciculate to form a large aggregate nerve which passes through an insertion slit to exit the shell plate and enter the underlying body tissues. (4) After traversing an insertion slit, the optic nerve defasciculates from other optic nerves to take an isolated pathway along the roof of the pallial cavity towards the lateral neuropil. (5) Upon contacting the lateral neuropil, the optic nerve splits to traverse two separate parallel tracts. (6) Each of these tracts travels bidirectionally along the lateral neuropil. The eyes of *A. granulata* have wide and overlapping visual fields and we propose different areas of the visual field (A–C) map to corresponding regions of the lateral neuropil (a–c) such that the lateral neuropil is structured as a visuotopic map.

tracts within the lateral neuropil that the separate sensory modality afferents could target, it is likely that sensory afferents of different modalities synapse with either the same or neighboring interneurons, which must then directly or indirectly mediate motor actions. It will be intriguing to learn how chitons guide their complex behaviors by efficiently constructing higher-order decentralized representations of multimodal sensory cues and then coordinating the multiplicity of these representations located around their bodies.

Sensory information processing in medullary cords

We have a poor understanding of sensory information processing in medullary cords such as the lateral neuropil of *A. granulata*, in large part because most of our knowledge about sensory information processing comes from studying neural circuits found in centralized ganglia. Well-studied neural circuits in molluscs tend to contain relatively large neurons with well-defined connections to each other (e.g. *Aplysia* swim reflex circuit; Hawkins et al., 1989), but the neural circuits found within medullary cords often include numerous small neurons with complex interconnections (Faller et al., 2012; Matsumura and Kuwasawa, 1996; Zullo et al., 2019). The small sizes of these neurons combined with their complex interconnections has made it difficult to apply conventional neurobiological techniques to understand the flow of information within medullary cords. Addressing this challenge will be a crucial step towards understanding how circuits within medullary cords process complex sensory information, such as that associated with spatial vision, polarization sensitivity and multimodal sensory inputs.

Our results suggest that the evolution of spatial vision in chitons involves changes to both sensory organs and neural architecture. Spatial vision in *A. granulata* appears linked to the evolution of image-forming eyes, as well as the subdivision of the lateral neuropil. How may a subdivided lateral neuropil contribute to visual processing in chitons? Optic neurites in *A. granulata* project to both tracts of the lateral neuropil, indicating these tracts do not represent modality-specific neural pathways. It is possible, however, that these tracts are associated with different sets of behaviors, e.g. motor responses that control defensive clamping responses versus those that control crawling. It is also possible that these tracts are

associated with the motor control of different tissues, e.g. muscle fibers in the girdle versus those in the foot. It is notable that the lateral neuropil of *C. tuberculatus*, a chiton with eyespots, resembles that of eyeless chitons in its lack of subdivision. Chitons with shell eyes and subdivided lateral neuropil, such as *A. granulata*, may have distributed visual systems that differ fundamentally from those of chitons with eyespots and undivided lateral neuropil, such as *C. tuberculatus*. From previous studies, we have learned that the visual systems of *A. granulata* and *C. tuberculatus* incorporate different light-sensing organs and provide information that informs different light-influenced behaviors (Speiser et al., 2011; Kingston et al., 2018). From the present study, we have learned that these distinct visual systems may be associated with different approaches to visual processing. Comparative studies of behavior and neuroanatomy, conducted within a phylogenetic framework, will help reveal more about the co-evolution of sensory organs, light-influenced behaviors and neural architectures within chitons.

Although we have a poor understanding of neural processing within medullary cords, they appear to be well suited for processing distributed sensory information and coordinating distributed motor control (Zullo et al., 2019). Among the most complex distributed sensory-motor networks are the bodies of octopuses, and running the length of each of the eight arms is a medullary cord (Shigeno et al., 2018). These medullary cords play an important role in the peripheral sensory-motor circuits, which octopuses rely on heavily to efficiently control their complex distributed hydrostatic bodies (Zullo et al., 2019). Chitons may be a simpler system in which to investigate the abilities and limits of decentralized cord-based processing because they lack the large brain found in octopuses. By studying distributed biological sensory processing networks such as the lateral neuropil of *A. granulata* and the medullary cords in the arms of octopuses, we may gain novel perspectives on effective and efficient ways to process large amounts of information generated in distributed sensor and information networks. Centralized networks often struggle with efficiency and coordination as they scale, and eventually centralized processing schemes become untenable (Sadler, 2005). Biological distributed processing networks, like those of chitons and cephalopods, may inspire solutions to this challenge because they have to maintain efficiency and effectiveness throughout ontogenetic scaling, and thus may offer unique insight into scale-invariant network topologies.

Acknowledgements
We thank Jeff Twiss for the use of his confocal microscope and Yakir Gagnon for inspiring the polarization trials. We also thank Alex Kingston for advice on the immunohistochemistry work and Fabienne Poulain for the use of her pressure microinjection setup.

Competing interests
The authors declare no competing or financial interests.

Author contributions
Conceptualization: D.R.C., D.I.S.; Methodology: D.R.C.; Software: D.R.C.; Validation: D.R.C., D.I.S.; Formal analysis: D.R.C.; Investigation: D.R.C.; Resources: D.I.S.; Data curation: D.R.C.; Writing - original draft: D.R.C., D.I.S.; Writing - review & editing: D.R.C., D.I.S.; Visualization: D.R.C.; Supervision: D.I.S.; Project administration: D.I.S.; Funding acquisition: D.I.S.

Funding
This research was supported, in part, by IOS award no. 1457148 from the National Science Foundation (to D.I.S.), an ASPIRE-I Track IV award from the Office of the Vice President for Research at the University of South Carolina (to D.I.S.), and a Grants-in-Aid of Research award from the Society for Integrative and Comparative Biology (to D.R.C.).

Data availability
All relevant data can be found within the article and its supplementary information.

References
Bates, D., Mächler, M., Bolker, B. and Walker, S. (2015). Fitting linear mixed-effects models using lme4. *J. Stat. Softw.* **67**, 1-48. doi:10.18637/jss.v067.i01
Bok, M. J., Nilsson, D.-E. and Garm, A. (2019). Photoresponses in the radiolar eyes of the fan worm *Acromegalomma vesiculosum*. *J. Exp. Biol.* **222**, jeb212779. doi:10.1242/jeb.212779
Boyle, P. R. (1969). Rhabdomeric ocellus in a chiton. *Nature* **222**, 895-896. doi:10.1038/222895a0
Brainard, D. H. (1997). The psychophysics toolbox. *Spat. Vision* **10**, 433-436. doi:10.1163/156856897X00357
Buehlmann, C., Mangan, M. and Graham, P. (2020). Multimodal interactions in insect navigation. *Anim. Cogn.* **23**, 1129-1141. doi:10.1007/s10071-020-01383-2
Chappell, D. R., Horan, T. M. and Speiser, D. I. (2021). Panoramic spatial vision in the bay scallop *Argopecten irradians*. *Proc. R. Soc. B Biol. Sci.* **288**, 20211730. doi:10.1098/rspb.2021.1730
Chelazzi, G., Della Santina, P. and Parpagnoli, D. (1987). Trail following in the chiton *Acanthopleura gemmata*: operational and ecological problems. *Mar. Biol.* **95**, 539-545. doi:10.1007/BF00393097
Dacke, M., Nilsson, D.-E., Scholtz, C. H., Byrne, M. and Warrant, E. J. (2003). Insect orientation to polarized moonlight. *Nature* **424**, 33. doi:10.1038/424033a
Faller, S., Rothe, B. H., Todt, C., Schmidt-Rhaesa, A. and Loesel, R. (2012). Comparative neuroanatomy of Caudofoveata, Solenogastres, Polyplacophora, and Scaphopoda (Mollusca) and its phylogenetic implications. *Zoomorphology* **131**, 149-170. doi:10.1007/s00435-012-0150-7
Fernandez, C., Vendrasco, M. and Runnegar, B. (2007). Aesthete canal morphology in twelve species of chiton (Polyplacophora). *Veliger* **49**, 51-69. doi:10.4003/0740-2783-25.1.51
Friedrich, L., Lam, W. S., Gordon, L., Smeets, P., Free, R., Brooker, L., Chipman, R. and Joester, D. (2021). Kaleidoscope eyes: microstructure and optical performance of chiton ocelli. *arXiv*. doi:10.48550/arXiv.2110.15199
Garm, A. and Mori, S. (2009). Multiple photoreceptor systems control the swim pacemaker activity in box jellyfish. *J. Exp. Biol.* **212**, 3951-3960. doi:10.1242/jeb.031559
Garm, A. and Nilsson, D.-E. (2014). Visual navigation in starfish: first evidence for the use of vision and eyes in starfish. *Proc. R. Soc. B Biol. Sci.* **281**, 20133011. doi:10.1098/rspb.2013.3011
Garm, A., Oskarsson, M. and Nilsson, D.-E. (2011). Box jellyfish use terrestrial visual cues for navigation. *Curr. Biol.* **21**, 798-803. doi:10.1016/j.cub.2011.03.054
Gould, S. J. (1997). The exaptive excellence of spandrels as a term and prototype. *Proc. Natl. Acad. Sci. USA* **96**, 10750-10755. doi:10.1073/pnas.94.20.10750
Gould, S. J. and Lewontin, R. C. (1979). The spandrels of San Marco and the Panglossian paradigm; a critique of the adaptationist programme. *Proc. R. Soc. B Biol. Sci.* **205**, 581-598. doi:10.1098/rspb.1979.0086
Haas, W. and Kriesten, K. (1978). Die Ästheten mit intrapigmentärem Schalenauge von *Chiton marmoratus* (Mollusca, Placophora). *Zoomorphologie* **90**, 253-268. doi:10.1007/BF01007694
Hawkins, R. D., Lalevic, N., Clark, G. A. and Kandel, E. R. (1989). Classical conditioning of the *Aplysia* siphon-withdrawal reflex exhibits response specificity. *Proc. Natl. Acad. Sci. USA* **86**, 7620-7624. doi:10.1073/pnas.86.19.7620
Hubrecht, A. A. W. (1882). Memoirs: a contribution to the morphology of the Amphinetura. *J. Cell Sci.* **s2-22**, 212-228. doi:10.1242/jcs.s2-22.86.212
Kingston, A. C. N., Chappell, D. R. and Speiser, D. I. (2018). Evidence for spatial vision in *Chiton tuberculatus*, a chiton with eyespots. *J. Exp. Biol.* **221**, jeb183632. doi:10.1242/jeb.183632
Kirwan, J. D., Bok, M. J., Smolka, J., Foster, J. J., Hernández, J. C. and Nilsson, D.-E. (2018). The sea urchin *Diadema africanum* uses low resolution vision to find shelter and deter enemies. *J. Exp. Biol.* **221**, jeb176271. doi:10.1242/jeb.176271
Larson, E. and Taulu, S. (2017). The importance of properly compensating for head movements during MEG acquisition across different age groups. *Brain Topogr.* **30**, 172-181. doi:10.1007/s10548-016-0523-1
Li, L., Connors, M. J., Kolle, M., England, G. T., Speiser, D. I., Xiao, X., Aizenberg, J. and Ortiz, C. (2015). Multifunctionality of chiton biomineralized armor with an integrated visual system. *Science* **350**, 952-956. doi:10.1126/science.aad1246
Marshall, J. and Cronin, T. W. (2011). Polarisation vision. *Curr. Biol.* **21**, R101-R105. doi:10.1016/j.cub.2010.12.012
Matsumura, S. and Kuwasawa, K. (1996). Both the heart and pericardium in the chiton *Acanthopleura japonica* receive dual innervation from the central nervous system. *Zoo. Sci.* **13**, 55-62. doi:10.2108/zsj.13.55
Mongeau, J.-M., Schweikert, L. E., Davis, A. L., Reichert, M. S. and Kanwal, J. K. (2021). Multimodal integration across spatiotemporal scales to guide invertebrate locomotion. *Integr. Comp. Biol.* **61**, 842-853. doi:10.1093/icb/icab041
Moseley, H. N. (1885). On the presence of eyes in the shells of certain chitonidae and on the structures of these organs. *Q. J. Microsc. Sci.* **25**, 37-60. doi:10.1242/jcs.s2-25.97.37

Nilsson, D.-E., Gislén, L., Coates, M. M., Skogh, C. and Garm, A. (2005). Advanced optics in a jellyfish eye. *Nature* **435**, 201-205. doi:10.1038/nature03484

Nowikoff, M. (1907). Uber die Rfickensinnesorgane der Placophoren nebst einigen Bemerkungen fiber die Schale derselben. *Z. Wiss. Zool.* **88**, 154-186.

Petralia, R. S., Yao, P. J., Kapogiannis, D. and Wang, Y.-X. (2021). Invaginating structures in synapses – perspective. *Front. Synaptic Neurosci.* **13**, 685052. doi:10.3389/fnsyn.2021.685052

Pignatelli, V., Temple, S. E., Chiou, T.-H., Roberts, N. W., Collin, S. P. and Marshall, N. J. (2011). Behavioural relevance of polarization sensitivity as a target detection mechanism in cephalopods and fishes. *Philos. Trans. R. Soc. Lond. B. Biol. Sci.* **366**, 734-741. doi:10.1098/rstb.2010.0204

Plate, L. H. (1897). *Die anatomie und phylogenie der chitonen. Zoologische Jahrbücher, Supplement 4 (Fauna Chilensis Erster Band)*, Vol. 1, pp. 1-243. Fischer.

Ramón Y Cajal, S. (1904). *La Textura del Sistema Nerviosa del Hombre y los Vertebrados*. Madrid: Moya.

Sadler, B. M. (2005). Fundamentals of energy-constrained sensor network systems. *IEEE Aerosp. Electron. Syst. Mag.* **20**, 17-35. doi:10.1109/MAES.2005.1499273

Schindelin, J., Arganda-Carreras, I., Frise, E., Kaynig, V., Longair, M., Pietzsch, T., Preibisch, S., Rueden, C., Saalfeld, S., Schmid, B. et al. (2012). Fiji: an open-source platform for biological-image analysis. *Nat. Methods* **9**, 676-682. doi:10.1038/nmeth.2019

Schmid, B., Schindelin, J., Cardona, A., Longair, M., Heisenberg, M. (2010). A high-level 3D visualization API for Java and ImageJ. *BMC Bioinformatics* **11**, 1-7. doi:10.1186/1471-2105-11-274

Shigeno, S., Andrews, P. L. R., Ponte, G. and Fiorito, G. (2018). Cephalopod brains: an overview of current knowledge to facilitate comparison with vertebrates. *Front. Physiol.* **9**, 952. doi:10.3389/fphys.2018.00952

Sigwart, J. D., Sumner-Rooney, L. H., Schwabe, E., Heß, M., Brennan, G. P. and Schrödl, M. (2014). A new sensory organ in 'primitive' molluscs (Polyplacophora: Lepidopleurida), and its context in the nervous system of chitons. *Front. Zool.* **11**, 7. doi:10.1186/1742-9994-11-7

Spagnolia, T. and Wilkens, L. A. (1983). Neurobiology of the scallop. II. Structure of the parietovisceral ganglion lateral lobes in relation to afferent projections from the mantle eyes. *Mar. Behav. Physiol.* **10**, 23-55. doi:10.1080/10236248309378605

Speiser, D. I., Eernisse, D. J. and Johnsen, S. (2011). A chiton uses aragonite lenses to form images. *Curr. Biol.* **21**, 665-670. doi:10.1016/j.cub.2011.03.033

Speiser, D. I., Demartini, D. G. and Oakley, T. H. (2014). The shell-eyes of the chiton *Acanthopleura granulata* (Mollusca, Polyplacophora) use pheomelanin as a screening pigment. *J. Nat. Hist.* **48**, 2899-2911. doi:10.1080/00222933.2014.959572

Speiser, D. I., Gagnon, Y. L., Chhetri, R. K., Oldenburg, A. L. and Johnsen, S. (2016). Examining the effects of chromatic aberration, object distance, and eye shape on image-formation in the mirror-based eyes of the bay scallop *Argopecten irradians*. *Integr. Comp. Biol.* **56**, 796-808. doi:10.1093/icb/icw099

Straka, H., Fritzsch, B. and Glover, J. C. (2014). Connecting ears to eye muscles: evolution of a 'simple' reflex arc. *Brain Behav. Evol.* **83**, 162-175. doi:10.1159/000357833

Sumner-Rooney, L. and Sigwart, J. D. (2018). Do chitons have a brain? New evidence for diversity and complexity in the polyplacophoran central nervous system. *J. Morph.* **279**, 936-949. doi:10.1002/jmor.20823

Sumner-Rooney, L., Rahman, I. A., Sigwart, J. D. and Ullrich-Lüter, E. (2018). Whole-body photoreceptor networks are independent of 'lenses' in brittle stars. *Proc. R. Soc. B Biol. Sci.* **285**, 20172590. doi:10.1098/rspb.2017.2590

Sumner-Rooney, L., Kirwan, J. D., Lowe, E. and Ullrich-Lüter, E. (2020). Extraocular vision in a brittle star is mediated by chromatophore movement in response to ambient light. *Curr. Biol.* **30**, 319-327. doi:10.1016/j.cub.2019.11.042

Towe, K. M. (1973). Trilobite eyes: calcified lenses in vivo. *Science* **179**, 1007-1009. doi:10.1126/science.179.4077.1007

Ullrich-Lüter, E. M., Dupont, S., Arboleda, E., Hausen, H. and Arnone, M. I. (2011). Unique system of photoreceptors in sea urchin tube feet. *Proc. Natl. Acad. Sci. USA* **108**, 8367-8372. doi:10.1073/pnas.1018495108

Von Knorre, H. (1925). Die Schale und die Rückensinnesorgane von *Trachydermon* (*Chiton*) *cinereus* L. und die ceylonischen Chitonen der Sammlung Plate. *Jenaische Zeitschrift für Naturwissenschaft* **61**, 469-632.

Zullo, L., Eichenstein, H., Maiole, F. and Hochner, B. (2019). Motor control pathways in the nervous system of *Octopus vulgaris* arm. *J. Comp. Physiol. A.* **205**, 271-279. doi:10.1007/s00359-019-01332-6

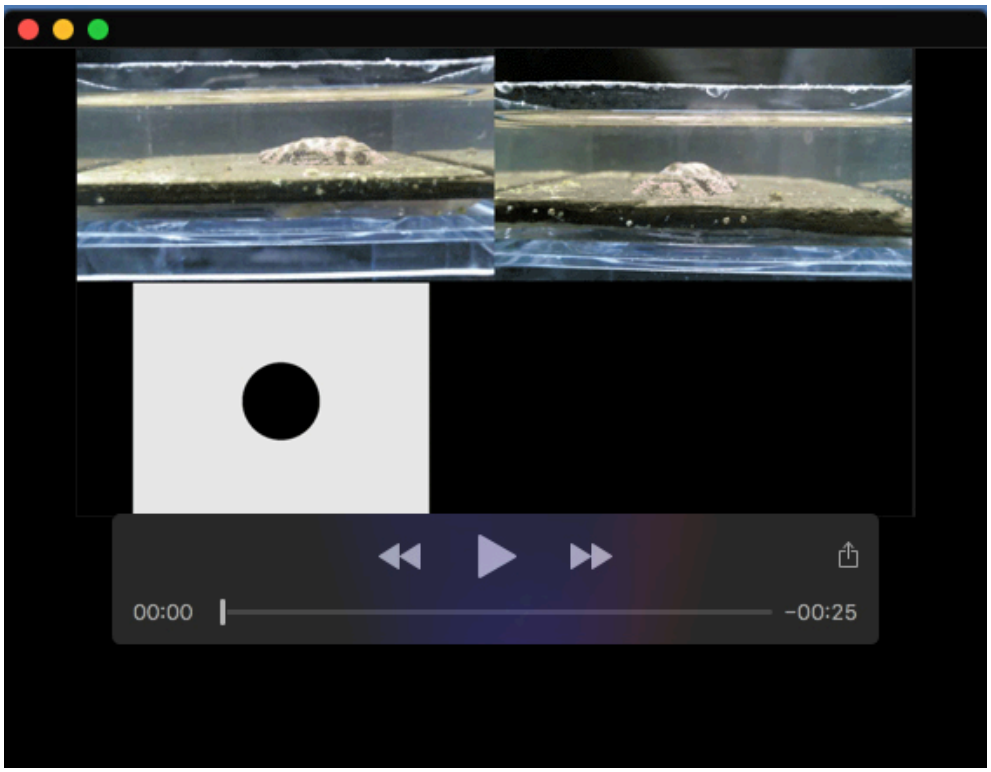

Movie 1. An example video recording of *A. granulata* behaviorally responding to the black-on-white loom. The video shows simultaneous orthogonal lateral views of the same chiton as well as a simultaneous screen recording of the overhead computer screen. In the beginning of the video, the chiton is slowly crawling towards the edge of the arena with sections of its girdle raised. When the looming black circle reaches a certain size, the chiton stops moving and lowers its girdle while simultaneously clamping to the substrate - which can be recognized by the lowering of the dorsal shell plates. This behavior is likely a defensive response, as the chiton is preparing itself for an impending attack by a looming predator.

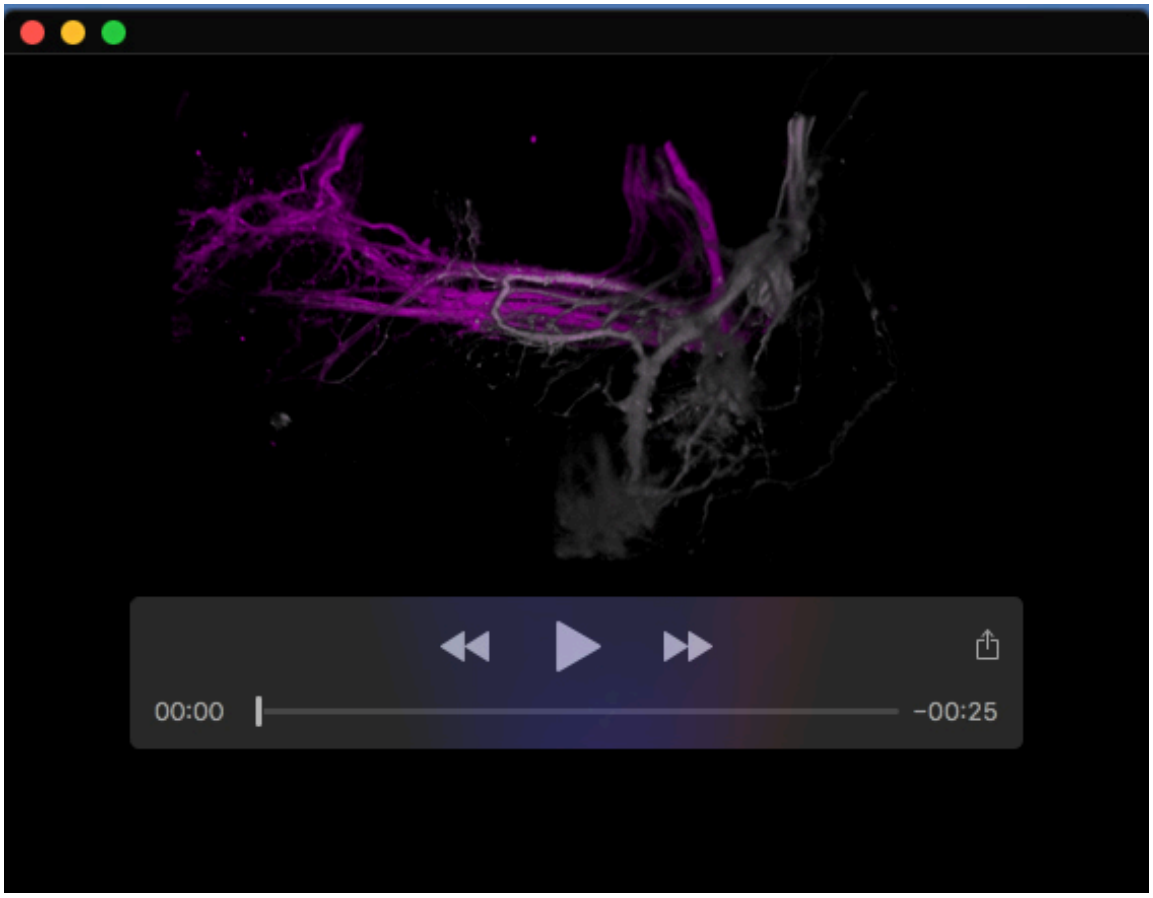

Movie 2. An animated 3-d reconstruction of the neural plexus of optic nerves along the lateral edge of a shell plate from *Acanthopleura granulata*. This video is a 3-d reconstruction of Fig. 4B, which is a composite maximum projection image. The relatively large white- and magenta-labeled nerves that converge on the underside of the neural plexus in the video correspond to the white and magenta arrows in Fig. 4B. The fluorescently labeled optic nerves traverse to the edge of the shell plate, where they exit the canal system and defasciculate to form a plexus. They then traverse this plexus to fasciculate and converge with other optic nerves at the site of an insertion slit before passing through the slit and reaching the underlying mantle tissue.

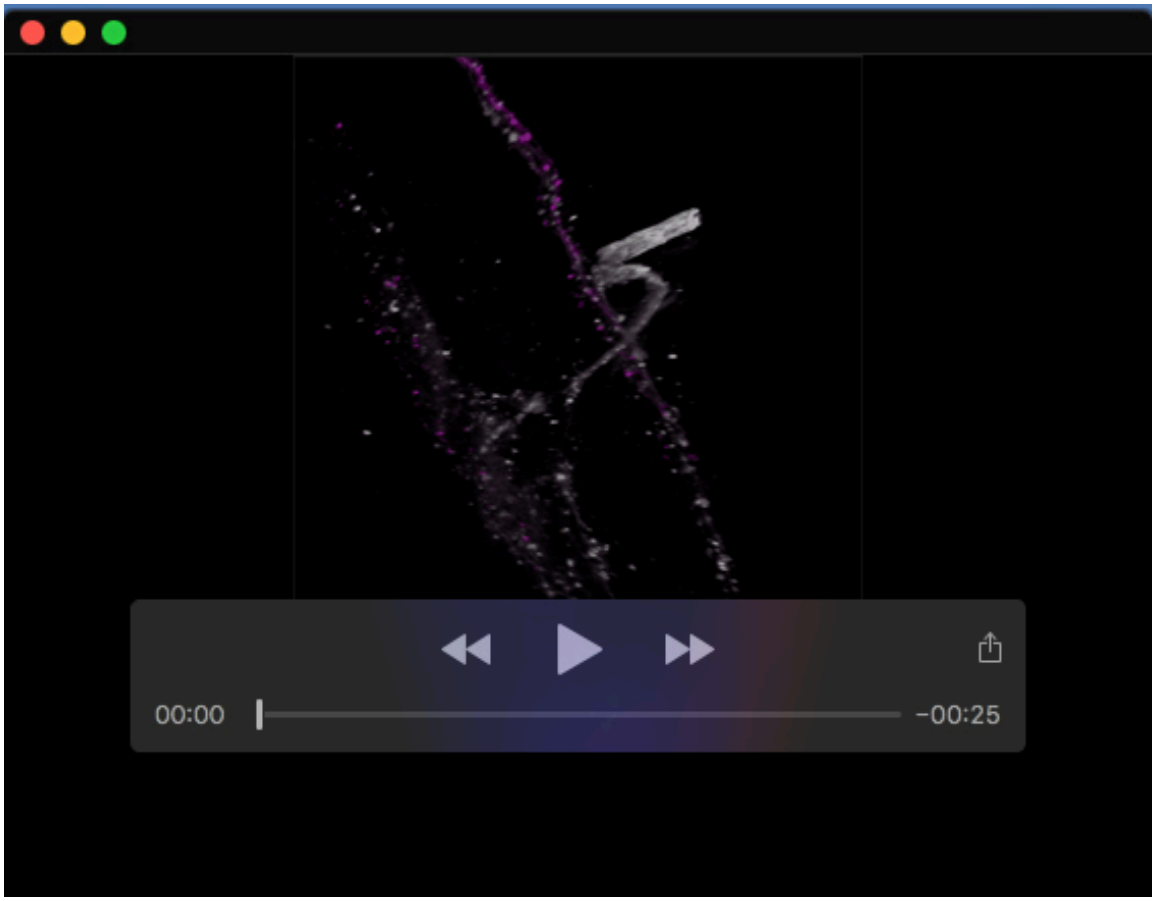

Movie 3. An animated 3-d reconstruction of the optic nerve arborization along the lateral neuropil of *Acanthopleura granulata.* This video is a 3-d reconstruction of the left section of Fig. 5C, which is a composite maximum projection image. The large white nerve in the video is the optic nerve labeled with a white arrow in Fig. 5C, and magenta neurites in the video are the traversing neurites of the optic nerve labeled with a magenta arrow in Fig 5C. The white fasciculated optic nerve splits into two separate neurite bundles which travel to separate tracts of the neuropil. The white- and magenta-labeled optic nerves are seen to travel in close proximity to one another and both have periodic varicosities that are likely *en passant* synapses.